Non-Markovian effects in the spin-boson model at zero temperature

S. Wenderoth [1], H.-P. Breuer [1,2] and M. Thoss [1,2]

[1] *Institute of Physics, University of Freiburg, Hermann-Herder-Strasse 3, D-79104 Freiburg, Germany*

[2] *EUCOR Centre for Quantum Science and Quantum Computing, University of Freiburg, Hermann-Herder-Strasse 3, D-79104 Freiburg, Germany*

(Received 22 January 2021; accepted 22 June 2021; published 19 July 2021)

We investigate memory effects in the spin-boson model using a recently proposed measure for non-Markovian behavior based on the information exchange between an open system and its environment. Employing the numerical exact multilayer multiconfiguration time-dependent Hartree approach, we simulate the dynamics of the spin-boson model at zero temperature for a broad range of parameters. For a fast bath, i.e., in the scaling limit, we find non-Markovian dynamics for a coherently decaying spin at weak system-bath coupling, whereas memory effects are absent for stronger coupling in the regimes of incoherent decay and localization. If the timescales of system and bath are comparable, a complex, nonmonotonic dependence of non-Markovianity on the system-bath coupling strength is observed.

DOI: 10.1103/PhysRevA.104.012213

I. INTRODUCTION

Open quantum systems are characterized by exchange of particles, energy, or information with an environment and are ubiquitous in physics and chemistry [1,2]. The coupling to the environment induces decoherence and dissipation, causing the relaxation of the system to an equilibrium or steady state. Besides these well-understood effects, the environment can also act as a memory for the open system leading to non-Markovian dynamics in the time evolution of the open system. Memory effects are often associated with the presence of a memory kernel in the Nakajima-Zwanzig equation for the reduced density matrix of an open quantum system [3–6]. However, a rigorous and representation-independent characterization and quantification of non-Markovianity in quantum systems is a highly topical and controversial issue (see, e.g., the reviews [7–9]).

In recent years, various mathematical and physical concepts have been developed in order to investigate quantum non-Markovianity. For example, definitions of non-Markovianity can be based on the divisibility properties of the underlying dynamical map, or on the correlations of the open system with an ancilla system [10–13]. Recently, a hierarchy of the different approaches to quantum non-Markovianity [14] and a generalization of the classical theory to the quantum regime based on quantum combs have been developed [15,16]. Here we will employ the physically motivated idea of using the flow of information between the open system and its environment in order to characterize quantum non-Markovianity [17,18]. The central quantity in this approach is the trace distance between two quantum states of the open system [19,20],

$$\mathcal{D}(\rho_1, \rho_2) = \tfrac{1}{2}\mathrm{Tr}|\rho_1 - \rho_2|, \tag{1}$$

where the modulus of an operator A is given by $|A| = \sqrt{A^\dagger A}$. This quantity can be interpreted as the distinguishability between the two states ρ_1 and ρ_2 [21]. Assuming that the initial state factorizes between the open system and the environment, the time evolution of the open system is determined by a family of completely positive and trace preserving (CPT) maps $\Phi(t)$. Any pair of initial states $\rho_{1,2}(0)$ then evolves into $\rho_{1,2}(t) = \Phi(t)\rho_{1,2}(0)$. The time-dependent trace distance is defined as

$$\mathcal{D}(t) = \mathcal{D}(\rho_1(t), \rho_2(t)). \tag{2}$$

Note that CPT maps are contractions for the trace distance, i.e., $\mathcal{D}(t) \leqslant \mathcal{D}(0)$ [22]. The CPT property alone, however, does not imply monotonicity of the trace distance as a function of time. If $\mathcal{D}(t)$ is a monotonically decreasing function of time and, hence, the two states $\rho_1(t)$ and $\rho_2(t)$ become less and less distinguishable, which can be interpreted as a continuous loss of information from the system to the environment, the dynamics is defined to be Markovian. Correspondingly, a temporal increase of the trace distance can be interpreted as a flow of information from the environment back to the open system, which is a unique signature of memory effects and, thus, of the non-Markovian character of the dynamics. On the basis of this interpretation one can define a measure for the degree of non-Markovianity of the dynamics as [17]

$$\mathcal{N} = \int_{\sigma>0} dt\, \sigma(t), \tag{3}$$

where $\sigma(t) = \frac{d}{dt}\mathcal{D}(t)$ and the integral extends over all time intervals in which $\sigma(t) > 0$. By definition, this measure is strictly zero if the trace distance decreases monotonically, i.e., if there is no information backflow from the environment to the system, which corresponds to Markovian dynamics. Such a behavior occurs, e.g., if the family of dynamical maps $\Phi(t)$

is CP-divisible [7]. The simplest and best known example is given by a dynamical semigroup with a time-independent generator in Lindblad form. We note that the trace distance also decreases monotonically for P-divisible processes which are thus Markovian in the above sense [12,23]. It is also noted that by maximization over the initial state pair the measure defined by Eq. (3) becomes a property of the dynamical map alone. In this work, however, we focus on a particular process defined by the dynamical map and the initial state pair.

II. MODEL

In this paper we employ the above discussed measure for non-Markovianity to investigate memory effects in the spin-boson model at zero temperature. To the best of our knowledge, this is the first systematic, nonperturbative (numerically exact) study of non-Markovianity in a nonintegrable model in the deep quantum regime at zero temperature [24]. Previous studies of non-Markovianity in the spin-boson model used perturbative approaches or focused on special parameter regimes such as higher temperature [25–29]. We also mention a path-integral study of non-Markovianity in a related model [30], albeit for finite temperature, and a very recent, similar investigation in the integrable model of quantum Brownian motion [31].

The spin-boson model, which involves a two-level system (or spin) interacting linearly with a bath of harmonic oscillators, is a paradigmatic model to describe dissipative quantum dynamics [1,32]. Despite its simple form, it has applications to a variety of different processes and phenomena, including electron transfer [33] and macroscopic quantum coherence [34]. On the other hand, the spin-boson model is also interesting from a more fundamental point of view as it shows a transition from coherent dynamics to incoherent decay as well as a quantum phase transition [35–37]. Here we focus on the unbiased spin-boson model. Employing mass-weighted coordinates, the Hamiltonian reads

$$H = \Delta\sigma_x + \frac{1}{2}\sum_n \left(p_n^2 + \omega_n^2 q_n^2\right) + \sigma_z \sum_n c_n q_n, \tag{4}$$

where σ_x and σ_z are the Pauli matrices, Δ denotes the coupling between the two spin states, and ω_n, q_n, and p_n represent the frequency, position, and momentum of the bath oscillators, respectively. The properties of the bath which influence the spin are summarized by the spectral density [1,32]

$$J(\omega) = \frac{\pi}{2}\sum_n \frac{c_n^2}{\omega_n}\delta(\omega - \omega_n). \tag{5}$$

Here we consider a spectral density of Ohmic form with an exponential cutoff [1,32]

$$J(\omega) = \frac{\pi}{2}\alpha\omega e^{-\frac{\omega}{\omega_c}}, \tag{6}$$

where α defines the coupling strength and ω_c denotes the characteristic frequency of the bath.

In the scaling limit ($\omega_c/\Delta \to \infty$), the dynamics of the spin can be grouped into three qualitatively different regimes, comprising coherent decay for weak system-environment coupling ($\alpha < 0.5$), incoherent decay (intermediate coupling, $0.5 < \alpha < 1$), and localization (strong coupling $\alpha > 1$). It is also known that for finite ω_c/Δ both critical couplings α shifts to larger values [24,37–39].

III. NUMERICAL METHOD

To simulate the dynamics of the spin-boson model, we use the multilayer multiconfiguration time-dependent Hartree approach (ML-MCTDH) [40–43] which allows us to propagate the wave function of the joint system in a numerically exact way. The ML-MCTDH approach represents a rigorous variational basis-set method, which uses a multiconfiguration expansion of the wave function, employing time-dependent basis functions and a hierarchical multilayer representation. Within this framework the wave function is expanded in terms of time-dependent configurations,

$$|\Psi(t)\rangle = \sum_{\mathbf{J}} A_{\mathbf{J}}(t)\prod_{n=1}^{N}|\phi_{j_n}^n(t)\rangle\,, \tag{7}$$

where $\mathbf{J}$ is a N-dimensional multi-index. Each configuration is a Hartree product of "single-particle" functions (SPFs) $|\phi_{j_n}^n(t)\rangle$, where N denotes the total number of single-particle (SP) degrees of freedom and n is the index of a particular SP group. Similar to the wave function, each SPF can be represented as a sum of time-dependent configurations. Continuing this expansion, the total wave function $|\Psi(t)\rangle$ is represented recursively in many layers, which corresponds to a hierarchical tensor decomposition in the form of a tensor tree network. Following the Dirac-Frenkel variational principle [44], the equations of motion are obtained from a variation of the wave function $|\Psi(t)\rangle$ with respect to the expansion coefficients of each layer [45]. A more detailed explanation of the ML-MCTDH method, including the expansion of the SPFs, and the equations of motion is presented in Appendix A. The ML-MCTDH approach allows for the simulation of large but finite quantum systems. Thus, we represent the continuous bath by a finite number of modes. In this work we use an equidistant distribution but other choices are possible [38,46]. To ensure convergence to the continuum limit over the timescale considered, we employ several hundreds of modes. For a detailed discussion of the numerical treatment of a continuous bath see Ref. [38].

IV. RESULTS

Using the ML-MCTDH approach, we investigate non-Markovian behavior in the spin-boson model. We focus on the low temperature regime, where non-Markovian effects are expected to be particularly pronounced [25]. To evaluate the time-dependent trace distance defined in Eq. (2), we simulate the dynamics for two different initial states of the spin. The reduced state of the spin is uniquely described by the Bloch vector $\mathbf{a}(t) = (\langle\sigma_x\rangle(t), \langle\sigma_y\rangle(t), \langle\sigma_z\rangle(t))^T$, where $\langle\sigma_i\rangle(t) = \langle\psi(t)|\sigma_i|\psi(t)\rangle$. Employing this representation, Eq. (2) can be expressed as

$$\mathcal{D}(t) = \tfrac{1}{2}|\mathbf{a}_1(t) - \mathbf{a}_2(t)|, \tag{8}$$

where $\mathbf{a}_{1(2)}(t)$ is the time-dependent Bloch vector corresponding to the first (second) initial state, respectively, and $|\mathbf{a}_1 - \mathbf{a}_2|$ denotes the Euclidean distance. It can be shown [47] that

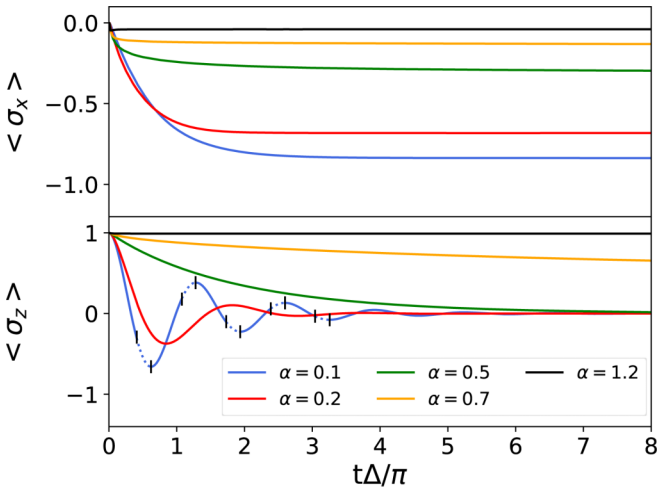

FIG. 1. Expectation value of σ_x and σ_z in the three different dynamical regimes of the spin-boson model for $\omega_c = 40\Delta$. For $\alpha = 0.1$ the first five non-Markovian intervals are marked by dashed lines.

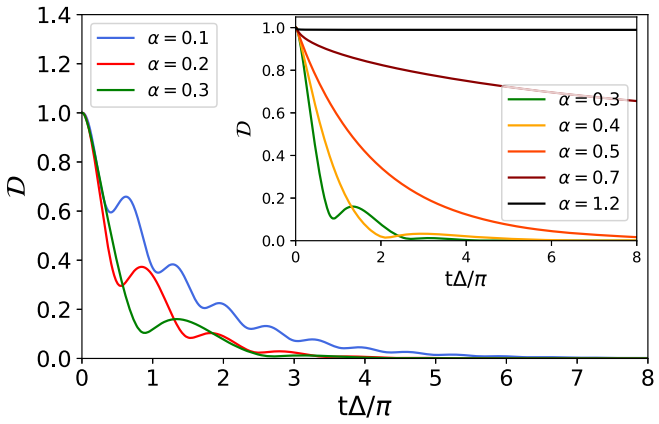

FIG. 2. Dynamics of the trace distance for different values of α and $\omega_c = 40\Delta$.

initial system states leading to a maximal non-Markovianity $\mathcal{N}$ must have the maximal initial trace distance $\mathcal{D}(0) = 1$ and, hence, must have orthogonal supports. For the present case of a two-state system (spin) this implies that the initial states must be a pair of pure orthogonal states (antipodal points on the Bloch sphere). Throughout this work we fix the initial states to the two eigenstates of σ_z, $\rho_1(0) = |\uparrow\rangle\langle\uparrow|$ and $\rho_2(0) = |\downarrow\rangle\langle\downarrow|$, which are often used in studies of the spin-boson model. The harmonic oscillators are initially all in the ground state and there is no correlation between the spin and the environment.

For the chosen initial states, the time evolution of $\mathbf{a}_2$ can be related to that of $\mathbf{a}_1$ (see Appendix B). Using this and the relation $\langle\sigma_y\rangle(t) = \frac{1}{2\Delta}\partial_t\langle\sigma_z\rangle(t)$, the trace distance can be written in terms of $\langle\sigma_z\rangle_1$ and its derivative as

$$\mathcal{D}(t) = \sqrt{[\langle\sigma_z\rangle_1(t)]^2 + \left[\frac{1}{2\Delta}\partial_t\langle\sigma_z\rangle_1(t)\right]^2}. \tag{9}$$

As a consequence of this equation, it follows that $\partial_t\langle\sigma_z\rangle_1(t_s) = 0$ implies $\partial_t\mathcal{D}(t_s) = 0$, i.e., if $\langle\sigma_z\rangle_1$ has a stationary point at t_s, the trace distance also has a stationary point at t_s. Note that the converse it not true.

For later analysis we note that in the weak coupling and large ω_c limit, an approximate analytic solution [1] for $\langle\sigma_z\rangle$ can be used to derive the following equation for the trace distance:

$$\mathcal{D}(t) = e^{-\gamma t}\sqrt{\tfrac{1}{2}[1+\eta] + \beta\sin(2\tilde{\Delta}t) + \tfrac{1}{2}[1-\eta]\cos(2\tilde{\Delta}t)}. \tag{10}$$

Here γ, $\tilde{\Delta}$, β, and η are constants which depend on the coupling strength α and on the characteristic bath frequency ω_c. The explicit expressions are given in Appendix C.

We begin our discussion of non-Markovian effects in the scaling regime, i.e., $\omega_c \gg \Delta$. As a starting point we recapitulate the dynamics of the spin and discuss the corresponding dynamics of the trace distance [1,32,38]. Figure 1 shows the dynamics of the spin for different values of the coupling strength α for $\omega_c = 40\Delta$, demonstrating the three qualitatively different dynamical regimes. Since $\langle\sigma_y\rangle(t) = \frac{1}{2\Delta}\partial_t\langle\sigma_z\rangle(t)$ holds, we only present the dynamics of $\langle\sigma_x\rangle$ and $\langle\sigma_z\rangle$.

In the weak coupling regime ($\alpha < 0.5$) the spin decays coherently to its stationary value. For increasing coupling strength, the oscillation frequency of $\langle\sigma_z\rangle$ decreases. The intermediate regime ($0.5 < \alpha < 1$) is characterized by a monotonic or incoherent decay of the spin. Upon increasing the coupling strength further, the decay slows down and eventually the spin localizes for coupling strengths larger than $\alpha = 1$. In all three regimes $\langle\sigma_x\rangle$ relaxes monotonously to its equilibrium value. For a more comprehensive discussion of the dynamics of the spin-boson model at zero temperature, see, e.g., Refs. [38,39].

Next we analyze the trace distance, which is the central object to quantify memory effects. Figure 2 shows the time-dependent trace distance for different values of the coupling strength α and $\omega_c = 40\Delta$. The behavior of the trace distance can be grouped into three different regimes, similar to the dynamics of the spin itself.

For weak coupling ($\alpha \lesssim 0.5$), the trace distance exhibits an overall decay to zero with periodic modulations including temporal increases, which indicate the presence of memory effects. For intermediate coupling in the incoherent regime of spin dynamics ($0.5 \lesssim \alpha \lesssim 1$), the trace distance decays monotonically. The decay slows down upon increasing coupling strength. In both regimes, the overall decay reflects a relaxation of the spin to an equilibrium state, where the equilibrium state is independent on the initial state.

In the following we discuss this non-Markovian regime in more detail. For a coherently decaying spin, $\langle\sigma_z\rangle(t)$ exhibits local minima and maxima and, thus, the trace distance $\mathcal{D}(t)$ has stationary points. Employing Eq. (10), it can be shown that these stationary points are all local maxima and, therefore, the non-Markovian intervals end at the extremal points of $\langle\sigma_z\rangle$. This is demonstrated in Fig. 1 for $\alpha = 0.1$. We find this behavior for all couplings $\alpha < 0.5$, as long as $\omega_c \gg \Delta$.

As the coupling strength approaches the coherent-to-incoherent transition ($\alpha = 0.5$), the renormalized frequency $\tilde{\Delta}$ vanishes, leading to a monotonically decaying spin.

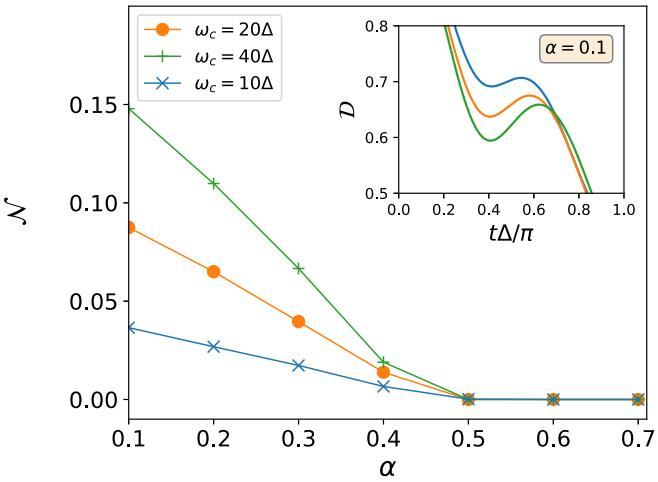

FIG. 3. Non-Markovianity $\mathcal{N}$ as a function of the coupling strength α for different characteristic frequencies ω_c. The symbols represent the data, the lines are a guide to the eye. The inset shows the first increase of the trace distance for different values of ω_c for $\alpha = 0.1$.

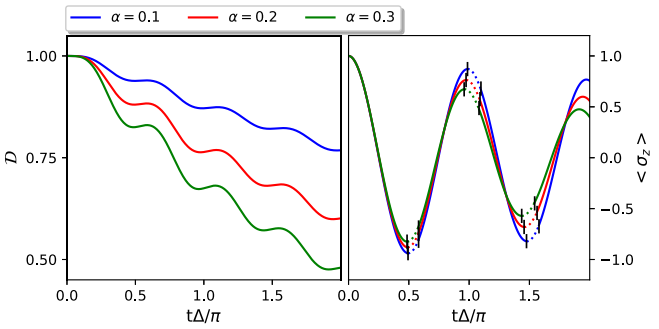

FIG. 4. Dynamics of the trace distance (left) and σ_z (right) for $\omega_c = \Delta$ in the weak coupling regime. For better visualization, only results for short times are shown. The non-Markovian intervals of σ_z are marked by dashed lines.

Additionally, the increases in the trace distance become weaker as $\alpha \to 0.5$. Thus, the non-Markovian intervals shift to infinite time and memory effects disappear as the dynamics changes from coherent to incoherent decay.

In order to quantify the non-Markovianity as a function of the coupling strength α, we use the cumulative measure $\mathcal{N}$ defined in Eq. (3). First note that without system-bath coupling (i.e., $\alpha = 0$), $\mathcal{D}(t) = 1$ holds for all times and, thus, $\mathcal{N} = 0$, as expected for a unitary time evolution. Figure 3 shows $\mathcal{N}$ as a function of the coupling strength α for different values of ω_c.

Because the trace distance exhibits memory effects in the regime of coherent decay, i.e., for $\alpha < 0.5$, the measure of non-Markovianity $\mathcal{N}$ is nonzero. In this regime the cumulative information backflow decreases monotonically as a function of the coupling strength. For $\alpha < 0.1$, the decay is too slow to obtain $\mathcal{N}$ directly from numerical simulations. Employing Eq. (10), which is valid in this weak-coupling regime, we find $\lim_{\alpha \to 0} \mathcal{N} = \mathcal{N}_0 > 0$ for fixed ω_c and, thus, the non-Markovianity is not analytic at $\alpha = 0$. The physical reason for this is that the relaxation time diverges as $\alpha \to 0$, and thus, memory effects are present at all times in this limit. The detailed derivation is provided in Appendix D, which also provides a discussion of the validity of perturbative methods such as the time-convolutionless master equation [25] to describe non-Markovian effects in the weak coupling regime (see Appendix E). For a monotonically decaying spin, i.e., for $\alpha \geqslant 0.5$, the trace distance also decays monotonically, and consequently, the non-Markovianity $\mathcal{N}$ vanishes.

We finish the discussion of the dynamics in the scaling regime with the influence of the time scale of the bath, determined by the characteristic frequency ω_c, on the non-Markovian behavior of the spin, illustrated in Fig. 3. For fixed α, the memory effects are more pronounced for larger characteristic bath frequencies as can be seen in the inset of Fig. 3. Consequently, the non-Markovianity $\mathcal{N}$ increases upon increasing the characteristic bath frequency. For all $\omega_c \geqslant 5\Delta$, we find a similar behavior of $\mathcal{N}$, i.e., $\mathcal{N}$ is nonzero only for $\alpha \leqslant 0.5$. Note that for $\omega_c = 5\Delta$ the non-Markovianity is almost zero ($\mathcal{N} < 0.01$) for all couplings α (data not shown).

In the following we discuss non-Markovian effects outside the scaling limit, focusing on the particularly interesting crossover regime $\omega_c \approx \Delta$, where the timescales of spin and bath are similar. For weak coupling α, depicted in Fig. 4 for the case $\omega_c = \Delta$, the overall dynamics are very similar to the scaling regime, i.e., the spin shows damped, coherent oscillations and the trace distance decays to zero with periodic modulations. The memory effects, however, exhibit a qualitatively different behavior. Unlike in the scaling regime, the non-Markovian intervals begin at the extremal points of $\langle \sigma_z \rangle$, indicating that $\mathcal{D}$ has local minima at the extremal points of $\langle \sigma_z \rangle$.

Further differences to the scaling regime are observed for stronger coupling α depicted in Fig. 5. The dynamics in this regime depends sensitively on ω_c and, therefore, we show results for different values of ω_c. Different to the scaling regime, the dynamics of the spin is partially coherent for $\alpha \geqslant 0.5$ (see also Refs. [24,38]), with an initial decay which does not slow down as the coupling strength is increased.

In addition, we find a qualitatively different non-Markovian behavior in the crossover regime $\omega_c \approx \Delta$. To demonstrate this, consider the first local minimum and maximum of $\langle \sigma_z \rangle$ for the case $\omega_c = 2\Delta$ in Fig. 5 (similar for $\omega_c = 3\Delta$). In the weak to moderate coupling regime (up to $\alpha \approx 0.7$), the stationary points of $\mathcal{D}$ associated with the two local extrema of $\langle \sigma_z \rangle$ are both local minima and, thus, both non-Markovian intervals begin at the local extrema. As the coupling strength is increased, the non-Markovian interval associated with the local maximum of $\langle \sigma_z \rangle$ first shrinks to zero and then extends to the left (i.e., to shorter times) with fixed end point at the local maximum of $\langle \sigma_z \rangle$. Eventually the two distinct intervals merge to a single non-Markovian interval extending from the local minimum to the local maximum. Upon further increasing the coupling strength, the initial decay becomes weaker and the following increase in the trace distance becomes smaller. This transition in the non-Markovian behavior results in a nonmonotonic dependence of the memory effects on the coupling strength α caused by this pair of extrema of $\langle \sigma_z \rangle$, i.e., memory effects first increase with α up to the point at which the two intervals merge and

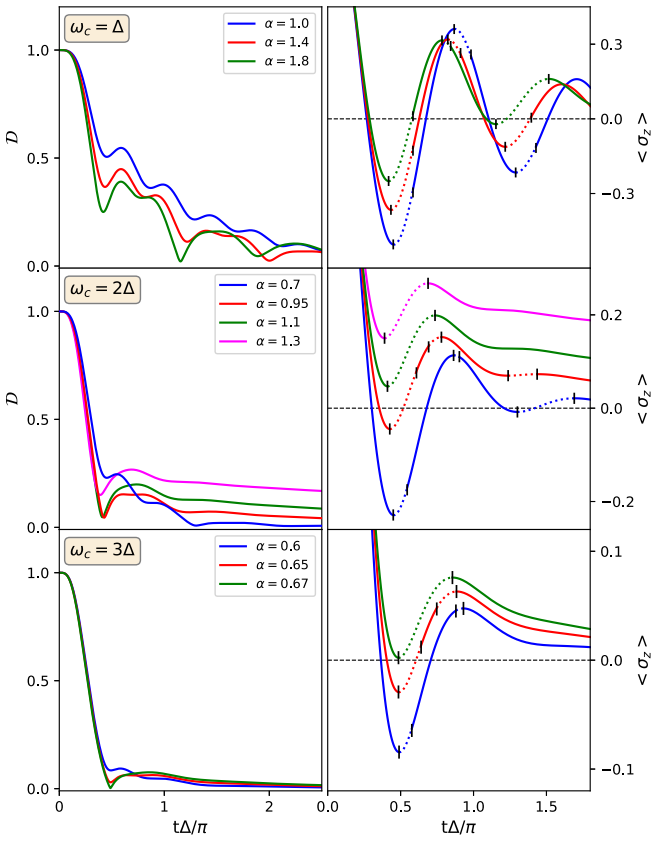

FIG. 5. Dynamics of the trace distance (left) and σ_z (right) for different characteristic frequencies ω_c in the moderate and strong coupling regime. The non-Markovian intervals are marked with dashed lines. For better visualization not all non-Markovian intervals are marked.

then decrease again. Similar transitions in the non-Markovian behavior are observed for later local extrema of $\langle\sigma_z\rangle$, albeit for weaker coupling α. For smaller ω_c, represented in Fig. 5 by the case $\omega_c = \Delta$, the first two non-Markovian intervals do not show such a transition and, therefore, memory effects increase monotonically with the coupling strength.

This dependence of memory effects on the coupling strength α is reflected in the cumulative measure for non-Markovianity $\mathcal{N}$ depicted in Fig. 6. For weak coupling α, $\mathcal{N}$ is very small for $\omega_c \in [2\Delta, 5\Delta]$, whereas it assumes

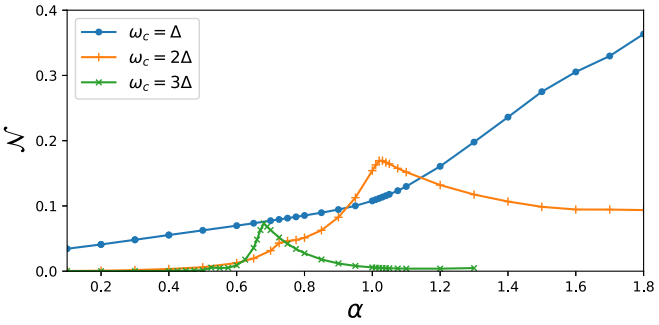

FIG. 6. Non-Markovianity $\mathcal{N}$ as a function of the coupling strength α for different characteristic frequencies ω_c.

significant values for $\omega_c = \Delta$. This is consistent with previous investigations of memory effects in the spin-boson model employing perturbative master equations, which predict Markovian dynamics if the effective spectral density of the environment is flat around the transition frequency of the spin [25], i.e., for $\omega_c = 2\Delta$. In the moderate and strong coupling regime, the transitions in the non-Markovian behavior discussed above give rise to different features in the non-Markovianity measure. For $\omega_c = 2\Delta$ and $\omega_c = 3\Delta$, the transition of the first local minimum and maximum of $\langle\sigma_z\rangle$ lead to a pronounced maximum of $\mathcal{N}$. Additionally, we find structures at $\alpha \approx 0.71$ and $\alpha \approx 0.52$ for $\omega_c = 2\Delta$ and $\omega_c = 3\Delta$, respectively, which coincide with the transition of non-Markovian behavior of the second local minimum and maximum of $\langle\sigma_z\rangle$. For $\omega_c = \Delta$, only the third oscillation of $\langle\sigma_z\rangle$ exhibits a transition at $\alpha \approx 1.4$, leading to a weak shoulder in the non-Markovianity $\mathcal{N}$. Otherwise $\mathcal{N}$ increases monotonically over the shown range of coupling strengths.

V. CONCLUSION

In summary we have employed the numerically exact ML-MCTDH approach to investigate non-Markovian effects in the spin-boson model at zero temperature. The results obtained for a broad range of parameters reveal a rich dynamical behavior. While in the scaling limit of a fast bath, the dynamics shows a transition from non-Markovian to Markovian as the decay of the spin changes from coherent to incoherent, the crossover regime without separation of timescales between spin and bath exhibits a complex, nonmonotonic dependence of non-Markovianity on the coupling strength. The question of how these findings can be generalized to more complex systems and an interacting bath as well as the dependence of non-Markovian effects on the initial state of the spin are interesting topics for future work.

ACKNOWLEDGMENTS

We thank Haobin Wang for providing the ML-MCTDH code used in this work and for many insightful discussions on quantum dynamics. This work was supported by the German Research Foundation (DFG) through IRTG 2079 and FOR 5099. Furthermore, support by the state of Baden-Württemberg through bwHPC and the DFG through Grant No. INST 40/575-1 FUGG (JUSTUS 2 cluster) is gratefully acknowledged.

APPENDIX A: DETAILS ABOUT THE NUMERICAL METHOD

The multilayer multiconfiguration time-dependent Hartree approach (ML-MCTDH) [40–43] is a well-established, accurate (numerically exact) method to simulate the dynamics of quantum systems with many degrees of freedom. It represents a rigorous variational basis-set method, which uses a multiconfiguration expansion of the wave function, employing time-dependent basis functions and a hierarchical multilayer representation. In the following we discuss the method in more detail and present some numerical aspects relevant for

(a)

$$|\Psi(t)\rangle = \sum_{\mathbf{J}} A_{\mathbf{J}}(t) \prod_{n=1}^{N} |\phi^n_{j_n}(t)\rangle\,, \tag{A1a}$$

$$|\phi^n_j(t)\rangle = \sum_{\mathbf{I}} B^{n,j}_{\mathbf{I}}(t) \prod_{q=1}^{Q(n)} |\nu^{(n,q)}_{i_q}(t)\rangle\,, \tag{A1b}$$

...

(b)

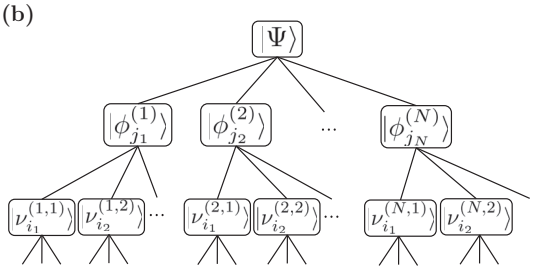

FIG. 7. (a) Expansion of the wave function $|\Psi\rangle$ and the first layer single-particle functions $|\phi^n_j\rangle$ used in the ML-MCTDH approach. (b) Tensor tree representation of the expansion. The time dependency is omitted for better visualization.

our calculations. For a more comprehensive discussion, see, e.g., [40,43].

Within the ML-MCTDH approach the time-dependent wave function is recursively expanded as depicted in Fig. 7. Here $A_{\mathbf{J}}(t)$, $B^{n,j}_{\mathbf{I}}(t)$, and so on are the expansion coefficients for the first, second, etc., layers, respectively; $|\phi^n_{j_n}(t)\rangle$, $|\nu^{(n,q)}_{i_q}(t)\rangle$, etc., are the single particle functions (SPFs) for the first, second, etc. layers. In Eq. (A1), N denotes the number of single particle (SP) groups in the first layer and $Q(n)$ denote the number of level two (L2) SP groups in the nth level one (L1) SP group. Such a recursive expansion can be carried out to an arbitrary number of layers. Finally, the multilayer hierarchy is terminated at a particular level by expanding the SPFs in the deepest layer in terms of time-independent basis functions/configurations, each of which may contain several physical degrees of freedom. The recursive expansion of the wave function $|\Psi(t)\rangle$ over many layers in the ML-MCTDH framework is a representation which corresponds to a hierarchical tensor decomposition in the form of a tensor tree network, shown in Fig. 7.

Following the Dirac-Frenkel variational principle [44], the equations of motion are obtained from a variation of the wave function $|\Psi(t)\rangle$ with respect to the expansion coefficients of each layer [40,43], resulting in

$$i\frac{\partial}{\partial t}\,|\Psi(t)\rangle_{\text{L1 coefficients}} = \hat{H}(t)\,|\Psi(t)\rangle\,, \tag{A2a}$$

$$i\frac{\partial}{\partial t}\,|\underline{\phi}^{(n)}(t)\rangle_{\text{L2 coefficients}} = \left[1-\hat{P}^{(n)}\right]\left[\hat{\rho}^{(n)}(t)\right]^{-1}\langle\hat{H}\rangle^{(n)}(t)\,|\underline{\phi}^{(n)}(t)\rangle\,, \tag{A2b}$$

$$i\frac{\partial}{\partial t}\,|\underline{\nu}^{(n,q)}(t)\rangle_{\text{L3 coefficients}} = \left[1-\hat{P}^{(n,q)}_{\text{L2}}\right]\left[\hat{\varrho}^{(n,q)}_{\text{L2}}(t)\right]^{-1}\langle\hat{H}\rangle^{(n,q)}_{\text{L2}}(t)\,|\underline{\nu}^{(n,q)}(t)\rangle\,, \quad \cdots\,, \tag{A2c}$$

where the SPFs for each group are summarized in a symbolic vector as $|\underline{\phi}^{(n)}(t)\rangle = \{|\phi^{(n)}_1(t)\rangle\,, |\phi^{(n)}_2(t)\rangle\,, \dots\}^T$ and analogously for the other SP groups. The time derivatives on the left-hand side are only performed with respect to the expansion coefficients of a particular layer (denoted by the respective subscript). $\hat{H}(t)$ represents the Hamiltonian matrix in terms of the first layer configurations, i.e.,

$$\left(\hat{H}(t)\right)_{\mathbf{JL}} = \left(\prod_{n=1}^{N}\langle\phi^n_{j_n}(t)|\right)\hat{H}\left(\prod_{n=1}^{N}|\phi^n_{l_n}(t)\rangle\right). \tag{A3}$$

In Eq. (A2) $\hat{\rho}^{(n)}(t)$ and $\hat{\varrho}^{(n,q)}_{\text{L2}}(t)$ are reduced density matrices for the first and second layers, respectively. The objects $\langle\hat{H}\rangle^{(n)}(t)$ and $\langle\hat{H}\rangle^{(n,q)}_{\text{L2}}(t)$ are mean-field operators for the first and second layer, respectively, and $\hat{P}^{(n)}$ and $\hat{P}^{(n,q)}_{\text{L2}}$ are SP-space projection operators for different layers. For the definition of these quantities we refer the reader to Ref. [43].

In this work we employ an implementation of the ML-MCTDH theory with up to four dynamical layers plus one static layer. To ensure that convergence is achieved, for each physical parameter a series of careful convergence tests were performed with respect to all the variational parameters such as the number of bath modes, primitive basis functions, and SPFs in each layer. In our calculations we employ 100–500 bath modes to faithfully represent the continuous distribution of bath modes over the timescale considered. For smaller characteristic bath frequencies ω_c, fewer modes (∼150) are required. The basis functions for each mode range from three (for high-frequency modes) to a few hundred (for low frequency modes). The number of SPFs in the highest layer ranges from 20 to 30, and in the lowest layer from 5 to 15, where the number of SPFs required for convergence increases with the coupling strength. The configuration space for each layer is typically a few hundred thousand.

APPENDIX B: MAPPING OF THE TIME EVOLUTION OF THE TWO DIFFERENT INITIAL STATES

The time-dependent trace distance for any pair of initial states of the spin can be calculated using

$$\mathcal{D}(t) = \frac{1}{2}\sqrt{\sum_{i=\{x,y,z\}}\left[\langle\sigma_i\rangle_1(t) - \langle\sigma_i\rangle_2(t)\right]^2}, \tag{B1}$$

where $\sigma_{x,y,z}$ denote the three Pauli matrices, and the index refers to the first and second initial state of the spin ρ_1 and ρ_2, respectively. The time-dependent expectation values in Eq. (B1) can be related to each other, which we will employ in the following. For the special choice of $\rho_1 = |\uparrow\rangle\langle\uparrow|$ and $\rho_2 = |\downarrow\rangle\langle\downarrow|$, in particular, the expectation values $\langle\sigma_i\rangle_1$ can be directly related to the expectation values $\langle\sigma_i\rangle_2$. In order to show this, we assume that the initial state of the joint system factorizes between the spin and the environment, and thus, can be written as

$$\varrho_1(0) = |\uparrow\rangle\langle\uparrow| \otimes \rho_B(0), \tag{B2}$$

$$\varrho_2(0) = |\downarrow\rangle\langle\downarrow| \otimes \rho_B(0), \tag{B3}$$

where $\rho_B(0)$ is the initial state of the environment. Formally, the time-dependent expectation values of the spin are

defined as

$$\langle\sigma_i\rangle_n = \mathrm{tr}\{\sigma_i e^{-iHt}\varrho_n(0)e^{iHt}\}, \tag{B4}$$

where $n \in \{1,2\}$, and H denotes the Hamiltonian of the full system given by

$$H = \Delta\sigma_x + H_B + \sigma_z\sum_n c_n q_n. \tag{B5}$$

Since $\sigma_x^2 = \mathbf{1}$ and $\sigma_x^\dagger = \sigma_x$ holds, the transformation $\tilde{O} = \sigma_x O \sigma_x$ is unitary. Expectation values are invariant under unitary transformations, and thus, Eq. (B4) can be transformed to

$$\begin{aligned}\langle\sigma_i\rangle_{1/2} &= \mathrm{tr}\{\sigma_x\sigma_i\sigma_x\sigma_x e^{-iHt}\sigma_x\sigma_x\rho_{1/2}(0)\sigma_x\sigma_x e^{iHt}\sigma_x\}\\ &= \mathrm{tr}\{\tilde{\sigma}_i e^{-i\tilde{H}t}\tilde{\rho}_{1/2}(0)e^{i\tilde{H}t}\}.\end{aligned} \tag{B6}$$

This transformation only acts on the Hilbert space of the spin, and thus, transforms only the spin operators. The transformed operators and initial state read

$$\sigma_x^\dagger\sigma_x\sigma_x = \sigma_x, \tag{B7}$$

$$\sigma_x^\dagger\sigma_y\sigma_x = -\sigma_y, \tag{B8}$$

$$\sigma_x^\dagger\sigma_z\sigma_x = -\sigma_z, \tag{B9}$$

$$\sigma_x\rho_1(0)\sigma_x = \rho_2(0). \tag{B10}$$

Inserting this into Eq. (B5) yields the transformed Hamiltonian

$$\tilde{H} = \sigma_x^\dagger H\sigma_x = \Delta\sigma_x + H_B + \sigma_z\sum_n(-c_n)q_n. \tag{B11}$$

The transformation only changes the sign of the couplings c_n.

The properties of the environment which influences the dynamics of the spin are fully characterized by the spectral density [1,32], which is defined as

$$J(\omega) = \frac{\pi}{2}\sum_n \frac{c_n^2}{\omega_n}\delta(\omega-\omega_n). \tag{B12}$$

Since the spectral density depends on the squared couplings, the two Hamiltonians H and $\tilde{H}$ give rise to the same spectral density. Consequently, the reduced spin dynamics induced by H and $\tilde{H}$ are equal. Using this and Eq. (B10) we conclude that

$$\langle\sigma_x\rangle_2(t) = \langle\sigma_x\rangle_1(t), \tag{B13}$$

$$\langle\sigma_y\rangle_2(t) = -\langle\sigma_y\rangle_1(t), \tag{B14}$$

$$\langle\sigma_z\rangle_2(t) = -\langle\sigma_z\rangle_1(t). \tag{B15}$$

Employing this result, Eq. (B1) can be expressed as

$$\mathcal{D}(t) = \sqrt{\langle\sigma_z\rangle_1^2 + \langle\sigma_y\rangle_1^2}. \tag{B16}$$

Here and in the following we suppress the time dependence of the expectation values. Finally, we employ that for the unbiased spin-boson model $\langle\sigma_y\rangle = \frac{1}{2\Delta}\partial_t\langle\sigma_z\rangle$ holds. With this we arrive at the final equation for the trace distance

$$\mathcal{D}(t) = \sqrt{\langle\sigma_z\rangle_1^2 + \frac{1}{(2\Delta)^2}[\partial_t\langle\sigma_z\rangle_1]^2}, \tag{B17}$$

from which one can calculate the derivative of the trace distance as

$$\partial_t\mathcal{D}(t) = \frac{[\partial_t\langle\sigma_z\rangle_1]\left[\langle\sigma_z\rangle_1 + \frac{1}{(2\Delta)^2}\partial_t^2\langle\sigma_z\rangle_1\right]}{\mathcal{D}(t)}. \tag{B18}$$

From this equation it directly follows that $\partial_t\langle\sigma_z\rangle = 0$ implies $\partial_t\mathcal{D} = 0$.

APPENDIX C: TRACE DISTANCE IN THE WEAK COUPLING REGIME

In the weak coupling and large ω_c limit, an approximate analytic solution [1] for $\langle\sigma_z\rangle(t)$ can be derived using a path integral approach. The time evolution of $\langle\sigma_z\rangle$ within this approach is given by

$$\langle\sigma_z\rangle(t) = e^{-\gamma t}\left[\cos(\tilde{\Delta}t) + \frac{\gamma}{\tilde{\Delta}}\sin(\tilde{\Delta}t)\right], \tag{C1}$$

where the renormalized frequency $\tilde{\Delta}$ and the damping γ depend on the characteristic bath frequency ω_c and the coupling strength α and are given by [1]

$$\tilde{\Delta} = [\Gamma(1-2\alpha)\cos(\pi\alpha)]^{\frac{1}{2(1-\alpha)}}\left(\frac{2\Delta}{\omega_c}\right)^{\frac{\alpha}{1-\alpha}}2\Delta, \tag{C2}$$

$$\gamma = \frac{\pi}{2}\alpha\tilde{\Delta}e^{-\frac{\tilde{\Delta}}{\omega_c}}. \tag{C3}$$

Using this result and Eq. (B17) an equation for the trace distance can be derived as

$$\mathcal{D}(t) = e^{-\gamma t}\sqrt{\tfrac{1}{2}[1+\eta] + \beta\sin(2\tilde{\Delta}t) + \tfrac{1}{2}[1-\eta]\cos(2\tilde{\Delta}t)}, \tag{C4}$$

where we defined the following constants:

$$\beta = \frac{\gamma}{\tilde{\Delta}}, \tag{C5}$$

$$\eta = \beta^2 + \frac{\tilde{\Delta}}{2\Delta}(1+\beta)^2. \tag{C6}$$

APPENDIX D: NONANALYTICITY OF THE NON-MARKOVIANITY

Equation (C4) can be used to further analyze the behavior of the non-Markovianity $\mathcal{N}$ in the weak coupling limit. First note that for $\alpha = 0$ the time evolution is unitary, and thus, $\mathcal{N} = 0$. To derive the behavior in the limit $\alpha \to 0$, we note that Eq. (C4) obeys

$$\mathcal{D}\left(t + \frac{\pi}{\tilde{\Delta}}\right) = e^{\frac{-\pi\gamma}{\tilde{\Delta}}}\mathcal{D}(t). \tag{D1}$$

Since this holds for all times t, the same holds for the derivative of the trace distance $\sigma(t) = \partial_t\mathcal{D}(t)$. Assuming that the non-Markovianity $\mathcal{N}$ is finite, which is true for all parameters considered here, the defining integral of $\mathcal{N}$ can be partitioned as

$$\mathcal{N} = \sum_{n=0}^{\infty}\int_{\substack{0\\ \sigma>0}}^{\pi/\tilde{\Delta}} dt\,\sigma\left(n\frac{\pi}{\tilde{\Delta}} + t\right). \tag{D2}$$

Employing property (D1) this can be written as

$$\mathcal{N} = \sum_{n=0}^{\infty} e^{-n\pi \frac{\gamma}{\tilde{\Delta}}} \int_{\substack{0 \\ \sigma > 0}}^{\pi/\tilde{\Delta}} dt\, \sigma(t), \tag{D3}$$

where the integral measures the information back flow during the first period of the time evolution. Let $I \subset [t, t + \frac{\pi}{\tilde{\Delta}}]$ denote the times at which $\sigma(t) > 0$. For simplicity we assume that I consists of a single, connected interval. This is true for the analytic solution given by Eq. (C4). In the following we denote with $t_{\min}$ and $t_{\max}$ the lower and upper end of the interval I, respectively. From the fundamental theorem of calculus it then follows that

$$\mathcal{N} = \sum_{n=0}^{\infty} e^{-n\pi \frac{\gamma}{\tilde{\Delta}}} [\mathcal{D}(t_{\max}) - \mathcal{D}(t_{\min})]. \tag{D4}$$

Since $\pi \frac{\gamma}{\tilde{\Delta}} > 0$ the geometric series can be resumed resulting in

$$\mathcal{N} = \frac{\mathcal{D}(t_{\max}) - \mathcal{D}(t_{\min})}{1 - e^{-\pi \frac{\gamma}{\tilde{\Delta}}}}. \tag{D5}$$

The nominator in Eq. (D5) accounts for memory effects occurring in the first period, whereas the denominator accounts for the remaining, periodically occurring, information back flows. The limit of the non-Markovianity as $\alpha \to 0$ can be obtained by considering the leading order behavior of the nominator and denominator, which read

$$\mathcal{D}(t_{\max}) - \mathcal{D}(t_{\min}) \sim -\alpha \left[\ln\left(\frac{2\Delta}{\omega_c}\right) + \gamma_{\mathrm{EM}} + \tfrac{\pi^2}{4} e^{-\frac{2\Delta}{\omega_c}} \right], \tag{D6}$$

$$1 - e^{-\pi \frac{\gamma}{\tilde{\Delta}}} \sim \alpha \frac{\pi^2}{2} e^{-\frac{2\Delta}{\omega_c}}. \tag{D7}$$

Since both terms are linear in α as $\alpha \to 0$, we conclude that

$$\mathcal{N} \sim -\frac{2}{\pi^2} e^{\frac{2\Delta}{\omega_c}} \left[\ln\left(\frac{2\Delta}{\omega_c}\right) + \gamma_{\mathrm{EMC}} + \frac{\pi^2}{4} e^{-\frac{2\Delta}{\omega_c}} \right], \tag{D8}$$

where γ_{EMC} denotes the Euler-Mascheroni constant. This shows that $\lim_{\alpha \to 0^+} \mathcal{N} > 0$, and thus, $\mathcal{N}$ is not analytic at $\alpha = 0$.

APPENDIX E: PERTURBATIVE TREATMENT OF THE DYNAMICS

Our numerically exact results allow for the validation of perturbative approaches and demonstrate certain limitations. Here we compare the numerically exact results with the analytic solution given by Eqs. (C1) and (C4) and results obtained with the time-convolutionless (TCL2) master equation approach [48,49]. The latter was previously used in Ref. [25] to investigate memory effects in the spin-boson model. In Fig. 8 the comparison of $\langle \sigma_z \rangle$ as well as the trace distance is shown for $\alpha = 0.1$ and $\alpha = 0.3$ for $\omega_c = 20\Delta$. For $\alpha = 0.1$ the TCL2 master equation approach, as well as the analytical equation, give qualitatively correct results for $\langle \sigma_z \rangle$ and $\mathcal{D}$. For the non-Markovianity we find $\mathcal{N} \approx 0.094$ from the TCL2 master equation approach and $\mathcal{N} \approx 0.095$ from the analytic solution. Both are close to the numerically exact value of $\mathcal{N} \approx 0.088$. Note that for $\alpha = 0.1$ we find this small overestimation of $\mathcal{N}$ within the two approximative approaches for all investigated values of $\omega_c > 10\Delta$.

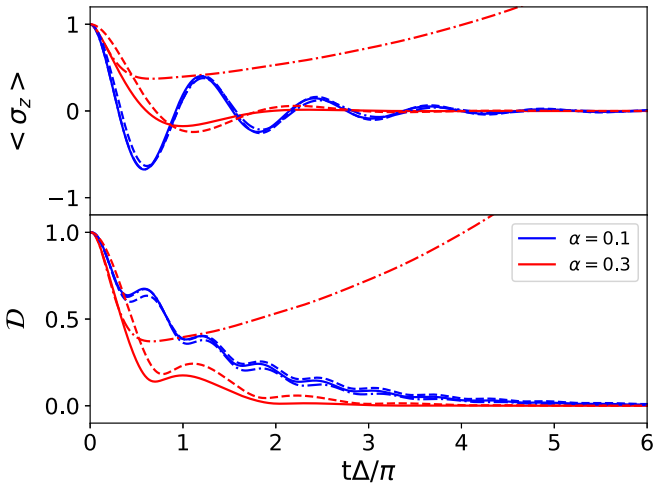

FIG. 8. Comparison between the numerically exact results (solid lines), the TCL2 master equation approach (dashed-dotted lines), and the analytical Eq. (C4) (dashed lines), for $\alpha = 0.1$ [blue (dark gray) curves] and $\alpha = 0.3$ [red (light gray) curves] for $\omega_c = 20\Delta$.

As the coupling strength increases, the approximations become less accurate and eventually break down. This is exemplified for $\alpha = 0.3$ in Fig. 8. The analytical solution still gives qualitatively good results, although the deviations from the numerically exact solution increases. For the non-Markovianity, it predicts $\mathcal{N} \approx 0.079$ compared to $\mathcal{N} \approx 0.041$ from the numerically exact simulations. The TCL2 approach, on the other hand, predicts unphysical results for longer times, in particular $\langle \sigma_z \rangle$ and $\mathcal{D}$ exceed one. This indicates that perturbation theory, as it is employed in the TCL2 method, is no longer valid for this value of the coupling strength. The analytical approach, on the one hand, uses renormalized perturbation theory, employing a resummation of all terms linear in the coupling strength of a path integral solution [1], and thus has a broader range of validity.

[1] U. Weiss, *Quantum Dissipative Systems*, 2nd ed. (World Scientific, Singapore, 1999).
[2] H.-P. Breuer and F. Petruccione, *The Theory of Open Quantum Systems* (Oxford University Press, Oxford, 2007).
[3] S. Nakajima, Prog. Theor. Phys. **20**, 948 (1958).
[4] R. Zwanzig, J. Chem. Phys. **33**, 1338 (1960).
[5] H. Mori, Prog. Theor. Phys. **33**, 423 (1965).
[6] L. Kidon, H. Wang, M. Thoss, and E. Rabani, J. Chem. Phys. **149**, 104105 (2018).
[7] H.-P. Breuer, E.-M. Laine, J. Piilo, and B. Vacchini, Rev. Mod. Phys. **88**, 021002 (2016).
[8] I. de Vega and D. Alonso, Rev. Mod. Phys. **89**, 015001 (2017).
[9] A. Rivas, S. F. Huelga, and M. B. Plenio, Rep. Prog. Phys. **77**, 094001 (2014).

[10] M. M. Wolf, J. Eisert, T. S. Cubitt, and J. I. Cirac, Phys. Rev. Lett. **101**, 150402 (2008).
[11] A. Rivas, S. F. Huelga, and M. B. Plenio, Phys. Rev. Lett. **105**, 050403 (2010).
[12] D. Chruściński, A. Kossakowski, and A. Rivas, Phys. Rev. A **83**, 052128 (2011).
[13] S. Luo, S. Fu, and H. Song, Phys. Rev. A **86**, 044101 (2012).
[14] L. Li, M. J. W. Hall, and H. M. Wiseman, Phys. Rep. **759**, 1 (2018).
[15] F. A. Pollock, C. Rodríguez-Rosario, T. Frauenheim, M. Paternostro, and K. Modi, Phys. Rev. A **97**, 012127 (2018).
[16] S. Milz and K. Modi, arXiv:2012.01894.
[17] H.-P. Breuer, E.-M. Laine, and J. Piilo, Phys. Rev. Lett. **103**, 210401 (2009).
[18] E.-M. Laine, J. Piilo, and H.-P. Breuer, Phys. Rev. A **81**, 062115 (2010).
[19] M. A. Nielsen and I. L. Chuang, *Quantum Computation and Quantum Information* (Cambridge University Press, Cambridge, England, 2000).
[20] M. Hayashi, *Quantum Information* (Springer, Berlin, 2006).
[21] C. A. Fuchs and J. van de Graaf, IEEE Trans. Inf. Theory **45**, 1216 (1999).
[22] M. B. Ruskai, Rev. Math. Phys. **06**, 1147 (1994).
[23] S. Wißmann, H.-P. Breuer, and B. Vacchini, Phys. Rev. A **92**, 042108 (2015).
[24] M. Thoss, H. Wang, and W. H. Miller, J. Chem. Phys. **115**, 2991 (2001).
[25] G. Clos and H.-P. Breuer, Phys. Rev. A **86**, 012115 (2012).
[26] H.-B. Chen, N. Lambert, Y.-C. Cheng, Y.-N. Chen, and F. Nori, Sci. Rep. **5**, 12753 (2015).
[27] A. Rivas, Phys. Rev. A **95**, 042104 (2017).
[28] M. Hinarejos, M.-C. Banuls, A. Perez, and I. de Vega, J. Phys. A: Math. Theor. **50**, 335301 (2017).
[29] A. Kurt and R. Eryigit, Phys. Rev. A **98**, 042125 (2018).
[30] C. A. Mujica-Martinez, P. Nalbach, and M. Thorwart, Phys. Rev. E **88**, 062719 (2013).
[31] S. Einsiedler, A. Ketterer, and H.-P. Breuer, Phys. Rev. A **102**, 022228 (2020).
[32] A. J. Leggett, S. Chakravarty, A. T. Dorsey, M. P. Fisher, A. Garg, and W. Zwerger, Rev. Mod. Phys. **59**, 1 (1987).
[33] R. A. Marcus and N. Sutin, Biochim. Biophys. Acta **811**, 265 (1985).
[34] U. Weiss, H. Grabert, and S. Linkwitz, J. Low Temp. Phys. **68**, 213 (1987).
[35] A. J. Bray and M. A. Moore, Phys. Rev. Lett. **49**, 1545 (1982).
[36] S. Chakravarty, Phys. Rev. Lett. **49**, 681 (1982).
[37] H. Wang and J. Shao, J. Phys. Chem. A **123**, 1882 (2019).
[38] H. Wang and M. Thoss, New J. Phys. **10**, 115005 (2008).
[39] H. Wang and M. Thoss, Chem. Phys. **370**, 78 (2010).
[40] H. Wang and M. Thoss, J. Chem. Phys. **119**, 1289 (2003).
[41] U. Manthe, J. Chem. Phys. **128**, 164116 (2008).
[42] O. Vendrell and H.-D. Meyer, J. Chem. Phys. **134**, 044135 (2011).
[43] H. Wang, J. Phys. Chem. A **119**, 7951 (2015).
[44] J. Frenkel, *Wave Mechanics* (Clarendon, Oxford, 1934).
[45] H. Wang and M. Thoss, J. Chem. Phys. **131**, 024114 (2009).
[46] I. de Vega, U. Schollwöck, and F. A. Wolf, Phys. Rev. B **92**, 155126 (2015).
[47] S. Wißmann, A. Karlsson, E.-M. Laine, J. Piilo, and H.-P. Breuer, Phys. Rev. A **86**, 062108 (2012).
[48] F. Shibata, Y. Takahashi, and N. Hashitsume, J. Stat. Phys. **17**, 171 (1977).
[49] S. Chaturvedi and F. Shibata, Z. Phys. B **35**, 297 (1979).